SCIENTIFIC REP🞄RTS

OPEN

Ultra-Wideband Impulse Radar Through-Wall Detection of Vital Signs

Xiaolin Liang[1], Jianqin Deng[1], Hao Zhang[2,3] & Thomas Aaron Gulliver[3]

This paper presents a new system for the detection of human respiration behind obstacles using impulse ultra-wideband (UWB) radar. In complex environments, low signal-to-noise ratios (SNRs) as they can result in significant errors in the respiration, heartbeat frequency, and range estimates. To improve the performance, the complex signal demodulation (CSD) technique is extended by employing the signal logarithm and derivative. A frequency accumulation (FA) method is proposed to suppress mixed products of the heartbeat and respiration signals and spurious respiration signal harmonics. The respiration frequency is estimated using the phase variations in the received signal, and a discrete short-time Fourier transform (DSFT) is used to estimate the range. The performance of the proposed system is evaluated along with that of several well-known techniques in the literature.

In recent years, the detection of living persons behind obstacles impulse ultra-wideband (UWB) radar has been investigated[1–5]. UWB radar has been used for the detection of humans[6,7], moving subjects[8,9], imaging in through-wall conditions[10,11], search and rescue[12,13], positioning indoors[14,15], and public order and security[16] because of its high range resolution and penetrability[17–20]. It can be used to detect human vital sign signals such as respiration and heart rates, but this can be difficult as thorax movement is usually only several millimeters, and the signal attenuation can be severe.

Previous researches on human vital sign detection have focused on suppressing stationary and/or nonstationary clutters, estimating the respiration frequency and heart rate, the analysis of signal characteristics, and other related problems[21–42]. The characteristics of human respiration signals were analyzed in both time and frequency domain[24,25] using the Hilbert-Huang transform (HHT) and fast Fourier transform (FFT). In[27], clutter similar to respiration signals was suppressed using adaptive clutter cancellation. In[28], the arctangent demodulation (AD) technique was employed in a UWB pulse radar system to accurately extract vital sign signals over long distances and in and through-wall conditions. However, this technique is complex and decreases the computational efficiency. A maximum likelihood estimator was considered in[29] to determine the period of vital sign signals under considering the additive-white-Gaussian-noise (AWGN). A post-processing algorithm was developed for respiration motion detection. The stationary and nonstationary clutters were removed by employing the singular-value-decomposition (SVD) algorithm when the signal-to-noise ratio (SNR) is low[30]. A tracing technique was considered to extract the respiration impulse response, but this approach is effective only when the SNR is high and over small distances[35]. LTS i.e. linear trend subtraction method was employed in[30] to reduce the linear trend. In[37], a higher order cumulants (HOC) technique was applied to extract vital sign signals considering that the fourth order cumulants of AWGN is zero. The classic EEMD i.e. ensemble empirical mode decomposition technique was used in[38] to estimate the heart rate of a living person by improving the SNR and removing clutter. An improved arctangent demodulation (AD) algorithm was proposed to increase the accuracies of human heart rate estimate[40]. In[42], a state-space method (SSM) was employed to extract vital sign signals including human respiration and heartbeat signals.

Most detection techniques are not effective over long distances and in through-wall conditions. To solve these problems, an algorithm based on UWB radar is developed here to calculate accurately vital sign signals in challenging environments. This is achieved by suppressing stationary, non-stationary and other clutter as well as the linear trend. The products of the vital sign signals and their harmonics are removed by employing a CSD-based

¹Science and Technology on Electronic Test & Measurement Laboratory, The 41st Research Institute of CETC, Xiang Jiang Road 98th, Qingdao, People's Republic of China. ²Department of Electronic Engineering, Ocean University of China, Song Ling Road 238th, Qing Dao, People's Republic of China. ³Department of Electrical Computer Engineering, University of Victoria, PO Box 1700, STN CSC, Victoria, BC, V8W 2Y2, Canada. Correspondence and requests for materials should be addressed to X.L. (email: iamxiaolin2016@126.com)
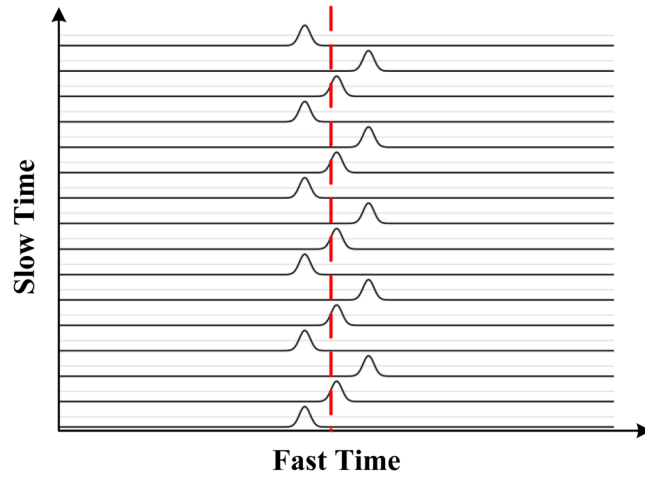
Figure 1. An illustration of the received pulses due to human respiration only.

frequency accumulation (FA) method. This is shown to perform better than several well-known techniques. The range information between human subject and radar is estimated considering the characteristics of vital sign signals and a discrete short-time Fourier transform (DSFT). Experimental results obtained using a UWB radar system at the Key Laboratory of Electromagnetic Radiation and Sensing Technology, Institute of Electronics, Chinese Academy of Sciences (IECAS), are used to evaluate the performance of the proposed technique.

The following parts of the paper are arranged as follows. The model of signal detection is given in Section 2, and the proposed method for vital sign detection is presented in Section 3. Section 4 provides performance results to evaluate the detection method, and the conclusions are presented in Section 5.

Signal Detection

Vital Sign Signal Model.   Vital sign signals may be obtained due to the time delay changes of a transmitted UWB pulse. The distance between human chest and radar is[32]

$$d(t) = d_0 + r(t) = d_0 + A_r \sin(2\pi f_r t) + A_h \sin(2\pi f_h t), \tag{1}$$

where the range between the radar and the center of human chest is given by d_0[30], f_r and A_r are the frequency and amplitude of human respiratory movement, respectively. f_h and A_h are the heart rate and heartbeat amplitude, respectively[32].

With only one human subject present in the detection environment and all other objects are considered as static, the impulse responses are

$$h(\tau, \ t) = a_v \delta(\tau - \tau_v(t)) + \sum_i a_i \delta(\tau - \tau_i), \tag{2}$$

where $\sum_i a_i \delta(\tau - \tau_i)$ represent the responses from all these static objects with time delay τ_i and vibration amplitude a_i[30], and $a_v \delta(\tau - \tau_v(t))$ represents the impulse response of the vital signs with amplitude a_v and time delay $\tau_v(t)$[32]. This delay is then

$$\tau_v(t) = \frac{2d(t)}{v} = \tau_0 + \tau_r \sin(2\pi f_r t) + \tau_h \sin(2\pi f_h t), \tag{3}$$

where $v = 3 \times 10^8$ m/s, $\tau_0 = 2d_0/v$, $\tau_r = 2A_r/v$, and $\tau_h = 2A_h/v$.

The signal received at the radar is then

$$R(\tau, \ t) = s(\tau) * h(t, \ \tau) = a_v s(\tau - \tau_v(t)) + \sum_i a_i s(\tau - \tau_i), \tag{4}$$

where $s(\tau)$ represents the transmitted pulse. $R(\tau, \ t)$ for a respiration signal is shown in Fig. 1. Slow-time represents the received pulse number and fast-time represents the range. In the signal model, t is slow-time with frequency components denoted by f, and τ is fast-time with frequency components denoted by v. The average human chest location is shown as a dashed line.

The discrete signal corresponding to (4) is

$$
\begin{aligned}
R[m, \ n] &= a_v s(m\delta_T - \tau_v(nT_s)) + \sum_i a_i s(m\delta_T - \tau_i) \\
&= a_v s(m\delta_R - v\tau_v(nT_s)) + \sum_i a_i s(m\delta_R - v\tau_i/2) \\
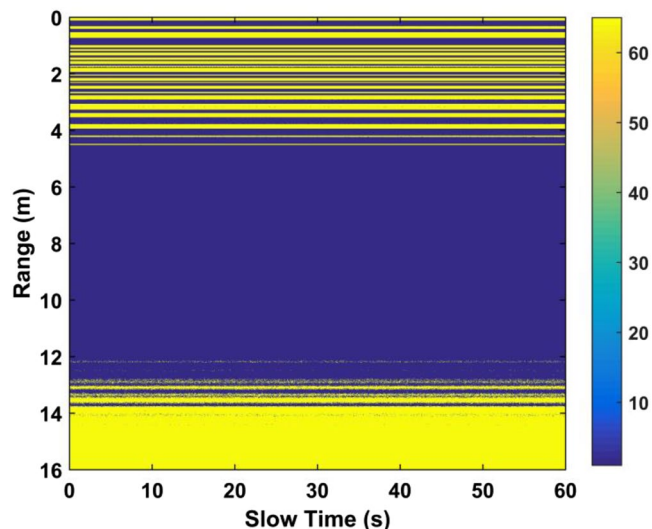&= h[m, \ n] + c[m],
\end{aligned} \tag{5}
$$

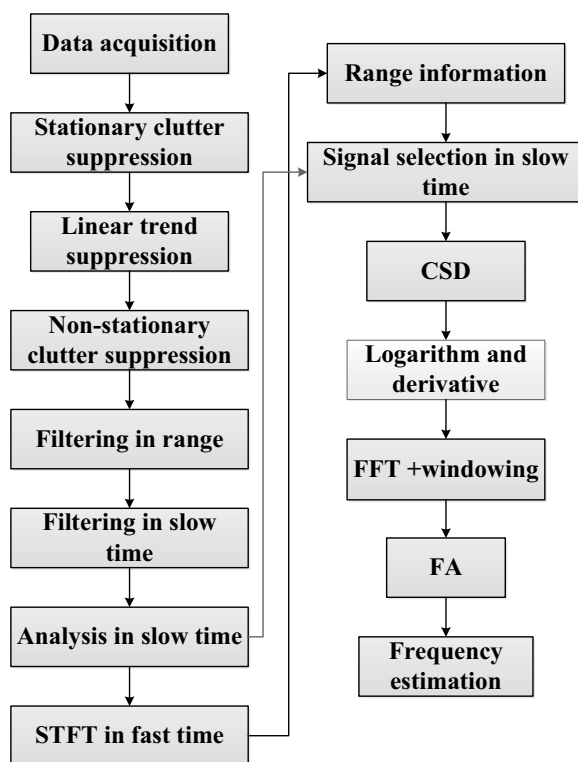**Figure 2.** The received UWB radar signal.

Figure 3. Flowchart of the proposed detection algorithm.

where $1/T_s$ represents the pulse repetition frequency (PRF), $t = nT_s, n = 0, \ldots, N - 1$ denote t samples, δ_T represents the sampling time in τ, $\delta_R = v\delta_T/2\, m = 0, \ldots, M - 1$ denote τ samples, $h[m, n]$ represent vital signs, and $c[m]$ represent static clutters. To avoid ambiguities in range and frequency aliasing, T_s should satisfy

$$1/T_s \geq 2(\max(f_r,\ f_h)). \tag{6}$$

In a real environment, (5) becomes

$$R_{M \times N} = h_{M \times N} + c_{M \times N} + a_{M \times N} + w_{M \times N} + q_{M \times N} + g_{M \times N} + z_{M \times N}, \tag{7}$$
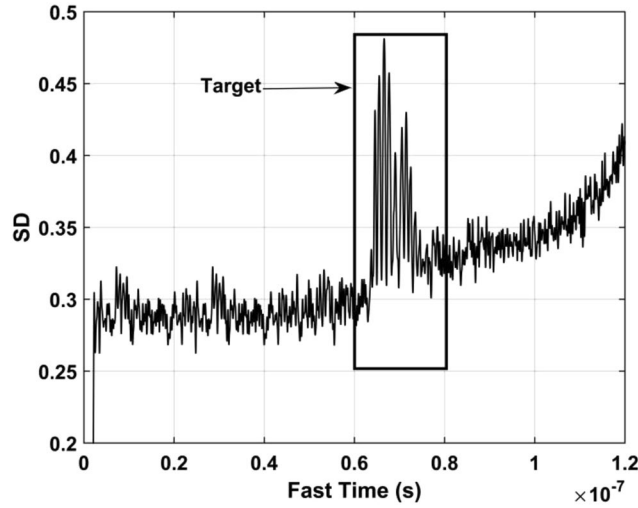
Figure 4. The SD obtained for a human subject outdoors located 9 m from the radar.

where $a_{M \times N}$ represents linear trend term, $w_{M \times N}$ represents AWGN, $q_{M \times N}$ represents non-stationary clutters, $g_{M \times N}$ represents unknown clutters, and $z_{M \times N}$ represents the clutters introduced by moving objects. A reflected pulse must be acquired within one pulse duration so that

$$T_w + \max\{\tau_v(t)\} - \min\{\tau_v(t)\} < T_s, \tag{8}$$

where T_w is the $-6\,\mathrm{dB}$ pulse width.

Vital Sign Signal Detection.   In static environments, the received pulses are shown in (4). Usually, the pulses without $c[m]$ are

$$\widetilde{R}(\tau, \; t) = a_v s(\tau - \tau_v(t)). \tag{9}$$

The frequencies of the vital sign signals are obtained by performing FT on $\widetilde{R}(m\delta_T, \; t)$ in t given by

$$Y(m\delta_T, \; f) = \int_{-\infty}^{+\infty} \widetilde{R}(m\delta_T, \; t) e^{-j2\pi ft} dt. \tag{10}$$

This can be acquired using the two-dimension FT of $Y(v, f)$ given by

$$Y(m\delta_T, \; f) = \int_{-\infty}^{+\infty} Y(v, \; f) e^{j2\pi v\tau} dv, \tag{11}$$

where

$$Y(v, \; f) = \int_{-\infty}^{+\infty} \int_{-\infty}^{+\infty} \widetilde{R}(m\delta_T, \; t) e^{-j2\pi ft} e^{-j2\pi v\tau} dt d\tau, \tag{12}$$
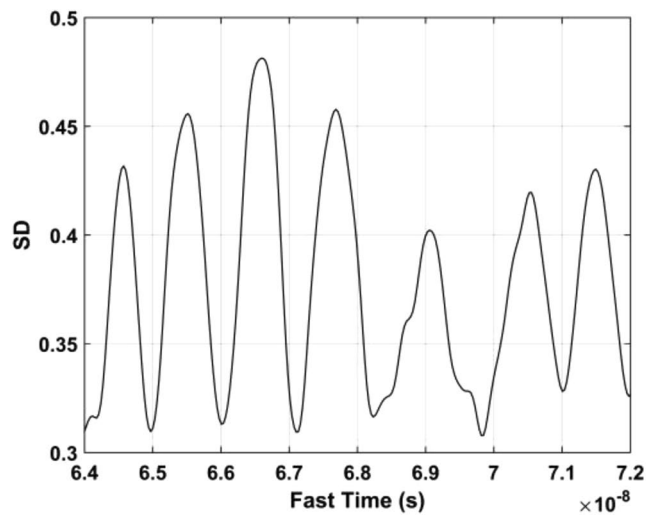
$$\begin{aligned} Y(v, f) &= \int_{-\infty}^{+\infty} a_v S(v) e^{-j2\pi ft} e^{-j2\pi v\tau_v(t)} dt, \\ &= a_v S(v) e^{-j2\pi v\tau_0} \int_{-\infty}^{+\infty} e^{-j2\pi v m_b \sin(2\pi f_r t)} e^{-j2\pi v m_h \sin(2\pi f_h t)} e^{-j2\pi ft} dt, \end{aligned} \tag{13}$$

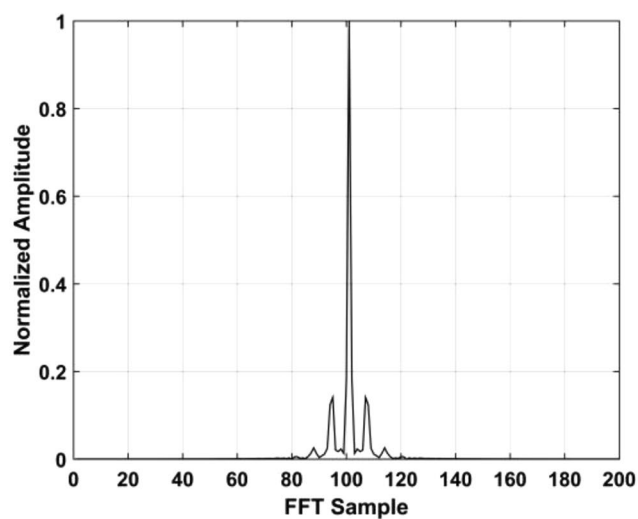and $S(v)$ is the FT of the transmitted UWB pulse. This can be represented using Bessel functions as

$$\begin{aligned} Y(v, \; f) &= a_v S(v) e^{-j2\pi v\tau_0} \\ &\times \int_{-\infty}^{+\infty} \left[\sum_{k=-\infty}^{+\infty} J_k(\beta_r v) e^{-j2\pi k f_r t} \right] \left(\sum_{l=-\infty}^{+\infty} J_l(\beta_h v) e^{-j2\pi l f_b t} \right) e^{-j2\pi ft} dt. \end{aligned} \tag{14}$$

$$e^{-jz \sin(2\pi f_0 t)} = \sum_{k=-\infty}^{+\infty} J_k(z) e^{-j2\pi k f_0 t}. \tag{15}$$

where $\beta_r = 2\pi A_r$ and $\beta_h = 2\pi A_h$.

Then, (10) is rewritten as

(a)

(b)

Figure 5. The SD in the target area in (**a**) the time-domain, and (**b**) the corresponding FFT.

$$Y(m\delta_T, \ f) = a_v \sum_{k=-\infty}^{+\infty} \sum_{l=-\infty}^{+\infty} G_{kl}(\tau)\delta(f - kf_r - lf_h).$$

(16)

where

$$G_{kl}(\tau) = \int_{-\infty}^{+\infty} S(\upsilon)J_k(\beta_r\upsilon)J_l(\beta_h\upsilon)e^{j2\pi\upsilon(\tau-\tau_0)}d\upsilon.$$
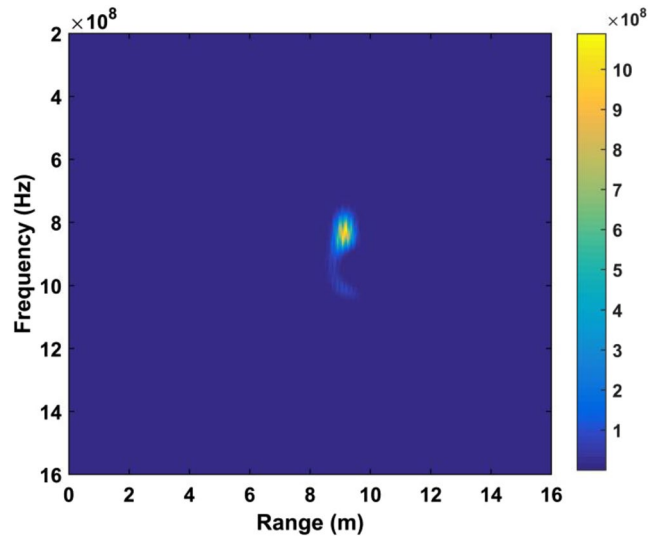
(17)

The maximum value of (17) can be obtained as

$$C_{kl} = G_{kl}(\tau_0) = \int_{-\infty}^{+\infty} S(\upsilon)J_k(\beta_r\upsilon)J_l(\beta_h\upsilon)d\upsilon$$
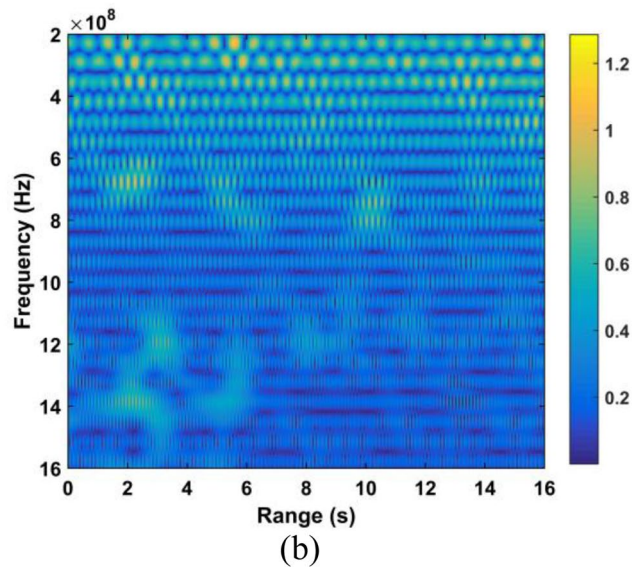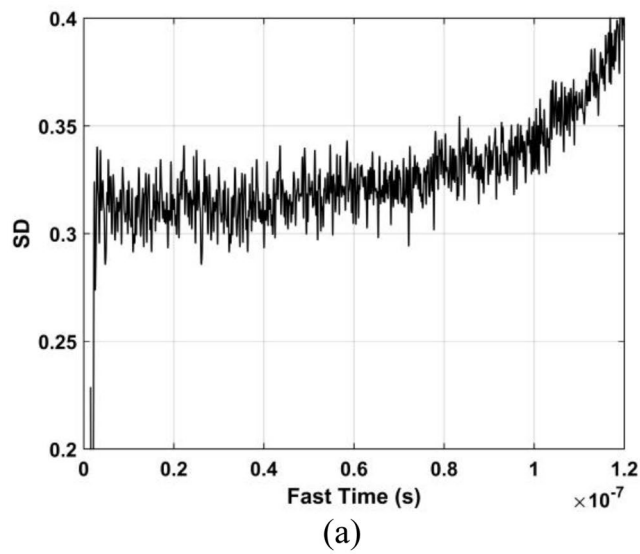
(18)

and setting $l = 0$ in

$$Y(\tau_0, \ f) = a_v \sum_{k=-\infty}^{+\infty} \sum_{l=-\infty}^{+\infty} C_{kl}\delta(f - kf_r - lf_h),$$
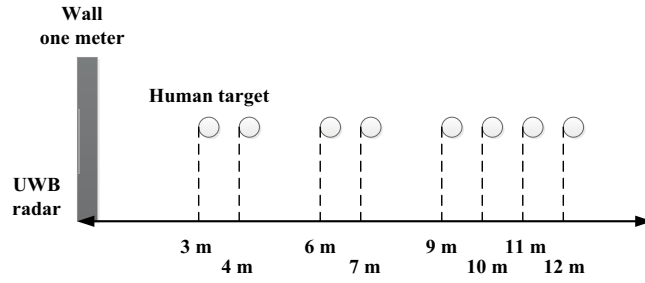
(19)

gives the respiration signal

Figure 6. The STFT for a human subject outdoors located 9 m from the radar.

(a)

(b)

Figure 7. Results without a human subject (**a**) the SD, and (**b**) the corresponding STFT.

Figure 8. The UWB radar experimental setup.

Figure 9. The experimental environment for a human subject (**a**) outdoors, and (**b**) indoors.

$$C_{k0} = \int_{-\infty}^{+\infty} S(v)J_k(\beta_r v)J_0(\beta_h v)dv. \tag{20}$$

setting $k = 0$ in (19), we can acquire the heartbeat signals as

$$C_{0l} = \int_{-\infty}^{+\infty} S(v)J_0(\beta_b v)J_l(\beta_h v)dv \approx \int_{-\infty}^{+\infty} S(v)J_l(\beta_h v)dv. \tag{21}$$

UWB Radar. The experimental data was obtained using a UWB radar with parameters given in[32]. The radar center frequency is 400 MHz and the PRF is 600 kHz. The UWB pulses were acquired form six segments simultaneously with a time window of 124 ns, $M_s = 682$ samples per segment, and $M = 4092$ fast-time samples. N_A samples are averaged to improve the SNR. Thus, a set of data is obtained every $M_s N_A/\text{PRF} = 34.1$ ms, and it takes 17.6 s to receive $N = 512$ pulses in slow-time. A combination of equivalent-time and real-time sampling[34] is employed as it provides better performance than equivalent-time sampling only[35].

Figure 2 shows the matrix R obtained using the UWB radar with a human subject at a distance of 9 m from the receiver in an outdoor environment which is described in Section IV. The vital sign signals are not evident due to the significant signal attenuation caused by the through-wall and long distance conditions. Thus, obtaining these signals in real environments is challenging, which motivates the development of a new method for vital sign detection.
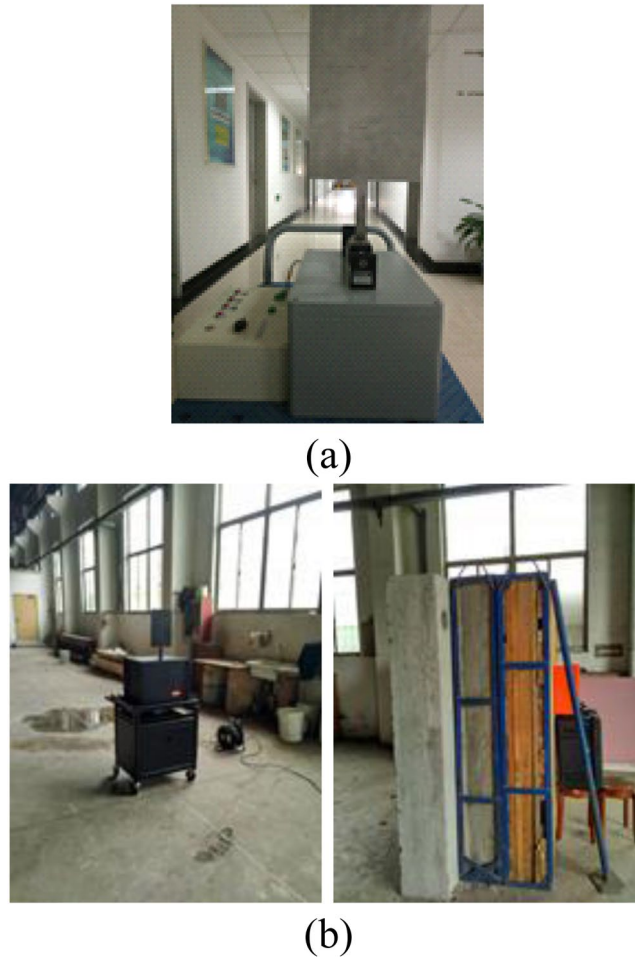
Figure 10. The actuator experiment (**a**) the actuator, and (**b**) the indoor environment.

Detection Algorithm

The new method for detection of the vital sign is designed in this section. A flowchart of this algorithm is given in Fig. 3. Two volunteers participated in this research. They were informed of the risks associated with participating in the experiments. This research was approved by both Ocean University of China and the Chinese Academy of Sciences. All experiments were performed in accordance with the relevant international guidelines and regulations.

Clutter Suppression. Respiration signals are typically corrupted by strong static clutters which are approximately slow-time invariant[30]. The DC component can be estimated as

$$\Im = \frac{1}{M \times N} \sum_{m=1}^{M} \sum_{n=1}^{N} R[m, \; n] \tag{22}$$

resulting in the matrix[31]

$$\Omega_{M \times N} = \Psi_{M \times N} - \Im \tag{23}$$

To further remove static clutter, range profile subtraction is employed which is[32]

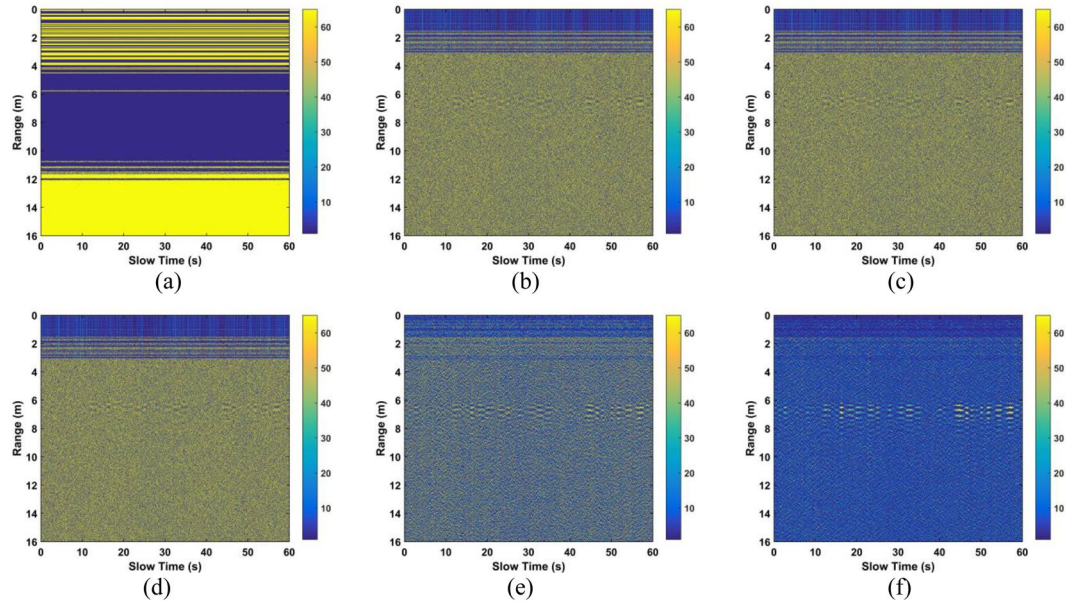$$\widehat{\Omega}[m, n] = \Omega[m, n] - \Omega[m, \; n - 1] \tag{24}$$

and then adaptive background subtraction is applied using a weighting coefficient λ to obtain

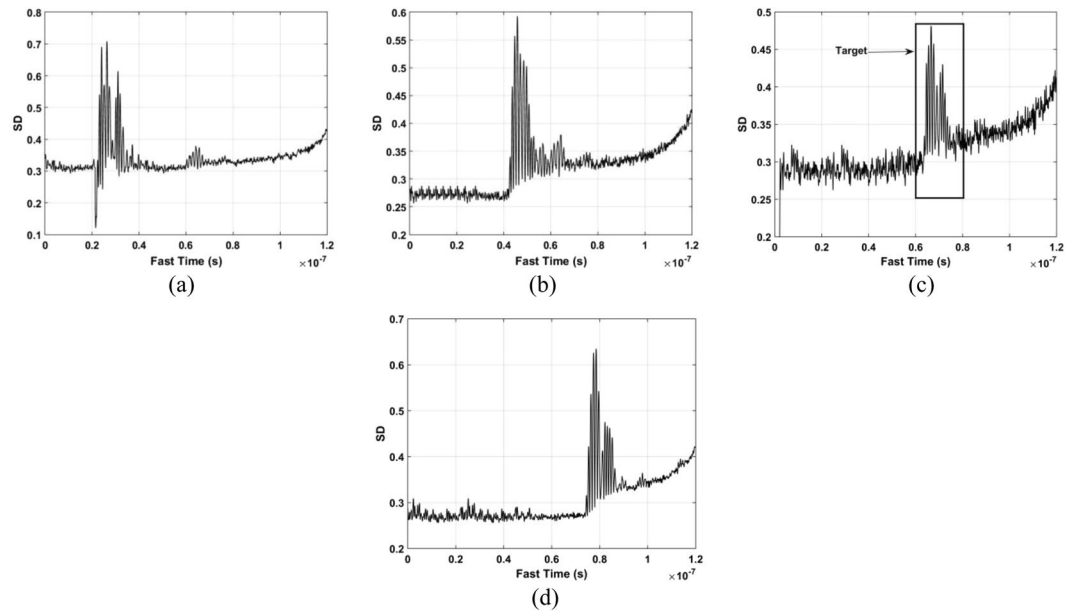$$p[m, \; n] = \lambda p[m, \; n - 1] + (1 - \lambda)\Omega[m, \; n] \tag{25}$$

which gives

$$T[m, \; n] = \Omega[m, \; n] - p[m, \; n] \tag{26}$$

Figure 11. The results after (**a**) TMS, (**b**) removing the stationary clutter, (**c**) LTS, (**d**) SVD, (**e**) filtering in fast-time, and (**f**) filtering in slow-time.

Figure 12. The SD for a subject outdoors located (**a**) 3 m, (**b**) 6 m, (**c**) 9 m, and (**d**) 11 m from the radar.

where $\lambda = 0.9$ and $p[m, 1] = \Omega[m, 1]^{43}$.

The LTS method estimates the linear trend $a_{M \times N}$ and removes it from the received pulses. A least-squares fit is used to eliminate $a_{M \times N}$ from the received pulses in slow-time by assuming that the starting point is a linear model for the received pulses. This can be expressed in matrix form as

$$T = X\beta \tag{27}$$

where $X = \left[\frac{k}{N} \quad 1_N \right], k = 0, 1, \ldots, N - 1$, and β denotes the unknown coefficient matrix which can be obtained by multiplying (27) by X^{T}

$$X^{\mathrm{T}} T = (X^{\mathrm{T}} X)\beta \tag{28}$$

Rearranging gives
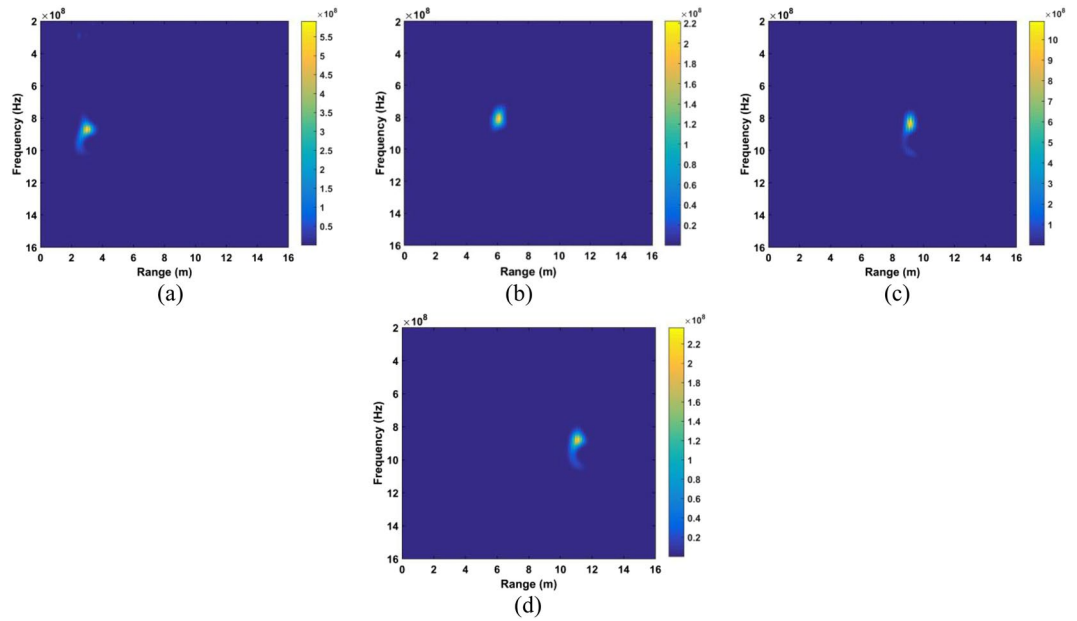
Figure 13. Range estimation using an STFT for a subject located (**a**) 3 m, (**b**) 6 m, (**c**) 9 m, and (**d**) 11 m from the radar.

Algorithm		Rang (m)			
		11	9	6	3
Proposed	Error (cm)	20	11	5	5
	Rate (Hz)	0.26	0.29	0.26	0.32
	SNR (dB)	3.25	3.67	4.32	7.58
CFAR	Error (cm)	954	672	436	27
	Rate (Hz)	0.46	0.72	0.10	0.18
	SNR (dB)	−15.3	−11.9	−7.22	−4.54
AM	Error (cm)	398	467	546	24
	Rate (Hz)	0.63	0.74	0.12	0.37
	SNR (dB)	−6.59	−3.69	0.84	5.35
MHOC	Error (cm)	725	156	243	35
	Rate (Hz)	0.44	0.52	0.45	0.14
	SNR (dB)	−11.4	−8.58	−5.85	−2.67

Table 1. Vital sign estimation with four methods.

$$(X^{T}X)^{-1}X^{T}T = \beta \tag{29}$$

Using (28) and (29), the linear trend can be calculated as

$$a = X\beta = X(X^{T}X)^{-1}X^{T}T \tag{30}$$

As a result, we can acquire the results given by

$$W = T - X(X^{T}X)^{-1}X^{T}T \tag{31}$$

In high SNR conditions, vital signs can easily be obtained even under $q_{M \times N}$ conditions. However, this clutter can significantly degrade signal estimation. SVD divides W into complementary subspaces which represent independent features of the received signal. This can be used to reduce the static/non-static clutter and increase the SNR. This decomposition is given by

$$W = USV^{T} \tag{32}$$

where S is a diagonal matrix, U is a $M \times M$ unitary matrix and V is a $N \times N$ unitary matrix. The elements of S are the singular values σ_i which are ranked in descending order, i.e. $\sigma 1 \geq \sigma 2 \geq \sigma 3 \geq \cdots \geq \sigma_r \geq 0$. The columns of
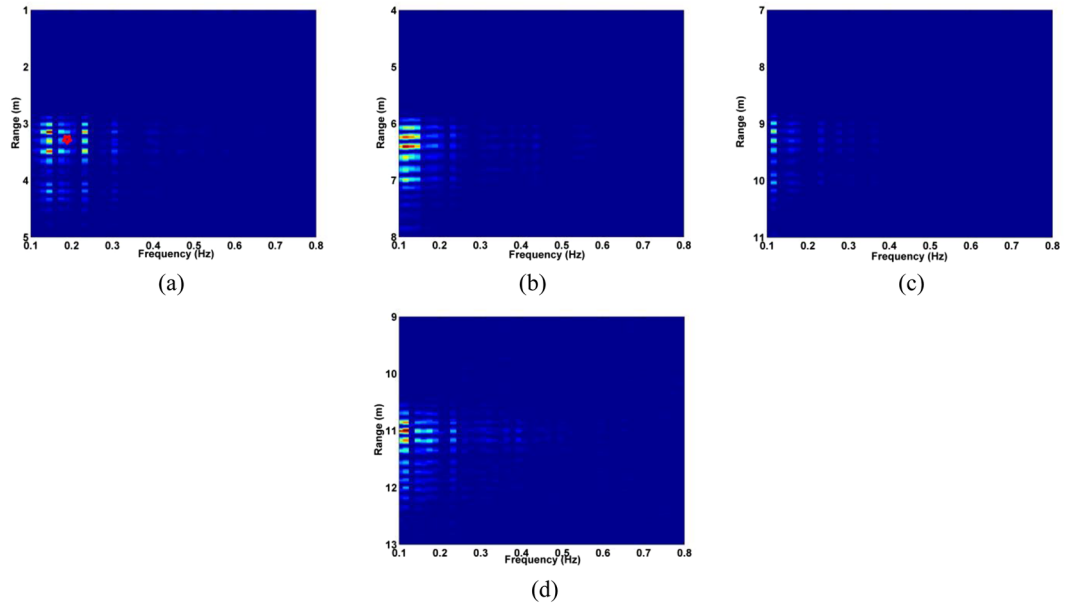
Figure 14. The range estimation using the CFAR method for a subject located (**a**) 3 m, (**b**) 6 m, (**c**) 9 m, and (**d**) 11 m from the radar.
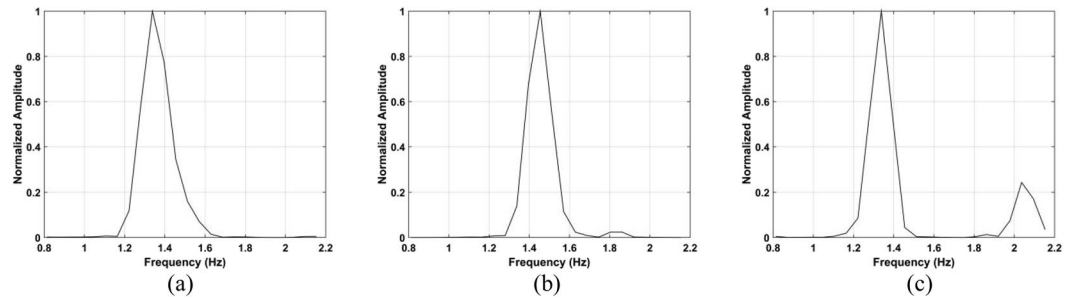
Figure 15. Heartbeat frequency estimation using the proposed method for a subject located (**a**) 3 m, (**b**) 6 m, and (**c**) 9 m from the radar.

Method	3 M	6 m	9 m
Proposed	6.57	4.22	1.23
CFAR	−3.56	−5.21	−12.6

Table 2. Heart rate detection SNR (dB) for the proposed and CFAR methods.

U are the left singular vectors and the columns of V are the right singular vectors. The eigenvectors of WW^{T} are U and the eigenvectors of $W^{\mathrm{T}}W$ are V.

The SVD in (32) can be expressed as

$$
\begin{aligned}
W &= \sigma_1 \begin{pmatrix} \vdots \\ \mu_1 \\ \vdots \end{pmatrix} (v_1 \ldots) + \sigma_k \begin{pmatrix} \vdots \\ \mu_k \\ \vdots \end{pmatrix} (\ldots v_k \ldots) + \cdots + \sigma_N \begin{pmatrix} \vdots \\ \mu_N \\ \vdots \end{pmatrix} (\ldots v_N \ldots) \\
&= M_1 + M_2 + \cdots + M_k + \cdots + M_G
\end{aligned}
\tag{33}
$$

where M_k is the kth intrinsic image with the same dimensions as W. The intrinsic images are arranged in descending order. M_1 is the first intrinsic image and is considered as $q_{M \times N}$. The images $M_2, M_3, \ldots, M_k$ typically contain the majority of the vital sign signals, while $M_{k+1}, \ldots, M_G$ mainly contain noise. Therefore, (33) can be rewritten as

$$
W = M_C + M_T + M_N
\tag{34}
$$
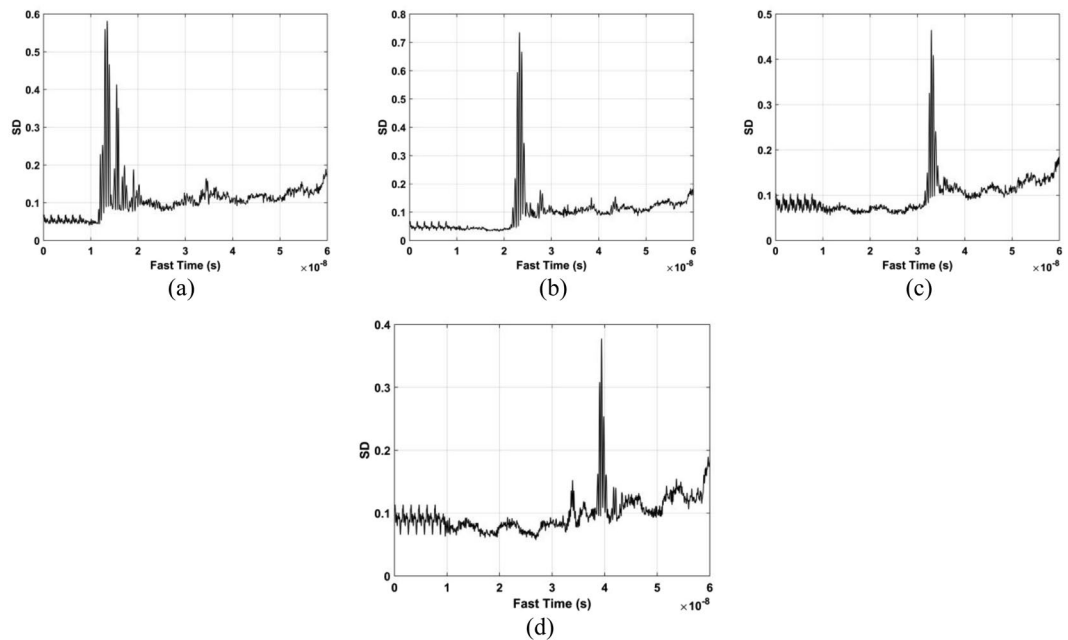
Figure 16. The SD for a subject indoors located (**a**) 4 m, (**b**) 7 m, (**c**) 10 m, and (**d**) 12 m from the radar.
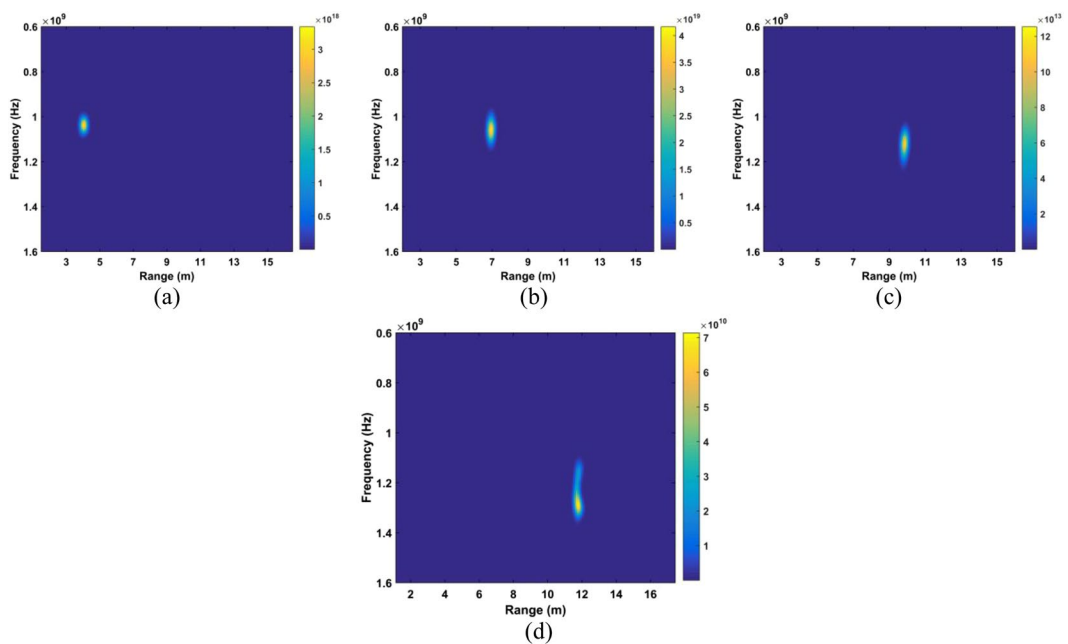
Figure 17. Range estimation using and STFT for a subject indoors located (**a**) 4 m, (**b**) 7 m, (**c**) 10 m, and (**d**) 12 m from the radar.

where M_C denotes $q_{M \times N}$, i.e. the first intrinsic image, M_T is the images containing the vital sign signals and M_N is the remaining images. SVD can be used to remove $q_{M \times N}$ which gives

$$\Phi = USV^{\mathrm{T}} = \sum_{i=2}^{G} u_i \sigma_{ii} v_i^{\mathrm{T}}$$

(35)

Note that it is difficult to estimate k so it is not possible to suppress the noise using this technique.
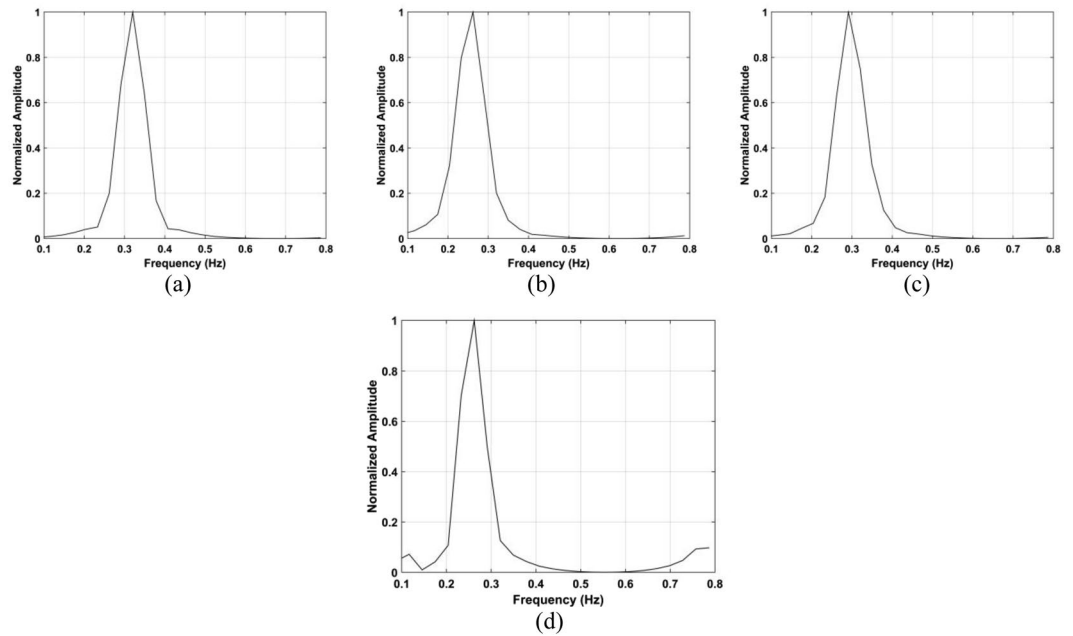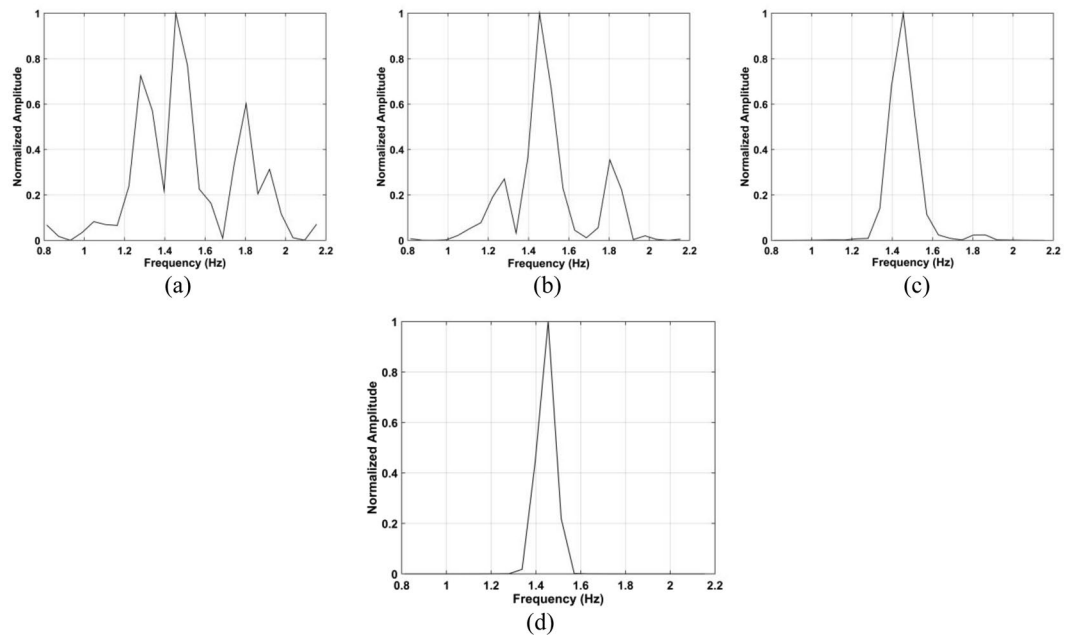
Figure 18. Respiration frequency estimation using the proposed method for a subject located (**a**) 4 m, (**b**) 7 m, (**c**) 10 m, and (**d**) 12 m from the radar.

Figure 19. Clutter suppression results using the FA method (**a**) once, (**b**) twice, (**c**) four times, and (**d**) six times.

SNR Improvement. The detection environment including the signal frequency can have a significant effect on the received signals[37]. As a result, the traditional matched filter maybe invalid for vital signs detection. Instead, a Butterworth bandpass filter (BPF) is employed which has transfer function[44]

$$|H(\omega)|^2 = \frac{1}{1 + (\omega/\omega_c)^{2N_f}} \tag{36}$$

where $N_f = 5$ is the filter order and ω_c is the cutoff frequency. This filter is composed of a Butterworth low pass filter (LPF) and a Butterworth high pass filter (HPF). This filter is used on (35) in the fast-time which gives
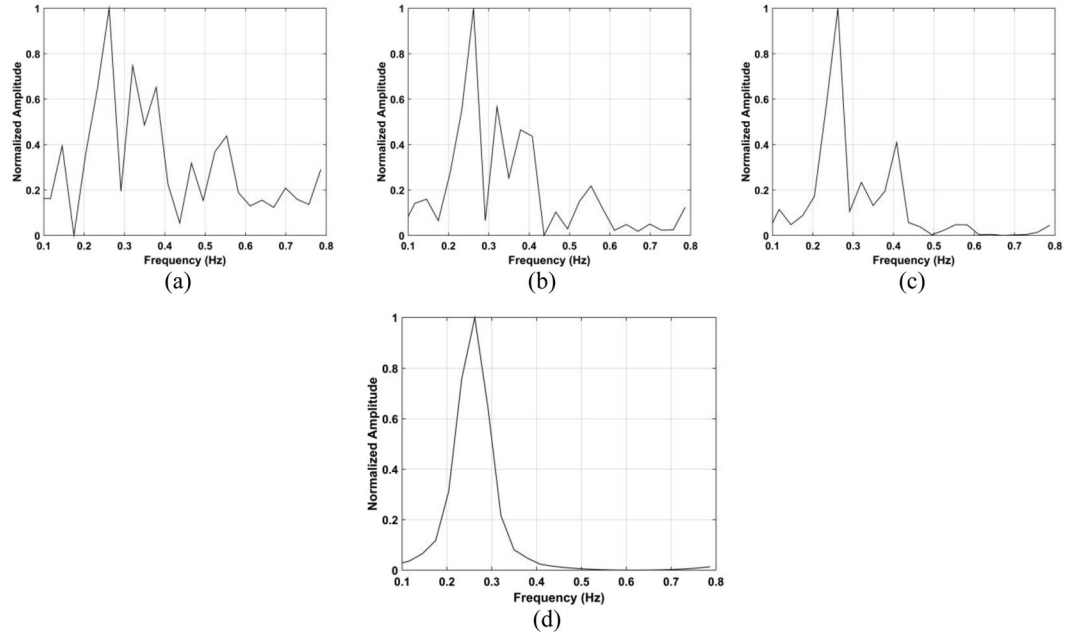
Figure 20. Clutter suppression results using the (**a**) FFT, (**b**) CSD-based one-FA, (**c**) CSD-based two-FA, and (**d**) CSD-based four-FA methods.

Method	SNR (dB)
FFT	0.39
CSD	0.23
LCSD	0.23
DLCSD	0.24
One FA	0.50
Two FA	1.26
Four FA	4.13
Six FA	4.36

Table 3. The SNR improvement with eight methods.

Method	1	2	3	Deviation (%)
FFT	0.29	0.11	0.23	36
CSD	0.29	0.46	0.11	39
LCSD	0.40	0.17	0.34	25
Proposed	0.34	0.34	0.34	4.7

Table 4. Frequency estimates with four methods.

$$\Lambda[m, \ n] \ = \ \chi_1 \Phi[m, \ n] + \chi_2 \Phi[m - 1, \ n] + ... + \chi_{N_b+1} \Phi[m - N_b, \ n]$$
$$- \kappa_2 \Phi[m - 1, \ n] - \cdots - \kappa_{N_a+1} \Phi[m - N_a, \ n] \tag{37}$$

where $N_b = N_a = 5, \kappa_i$ and χ_i are the filter coefficients.

An average extraction filter is now used to eliminate low- and high-frequency clutter. The output is

$$\Psi[k, \ n] = \frac{1}{\beta} \sum_{m=\beta k}^{\beta(k+1)-1} \Lambda[m, \ n], \tag{38}$$

where $k = 1, \ \ldots, \ \lfloor M/\beta \rfloor, \beta = 7$ is the number of filter coefficients, $\lfloor M/\beta \rfloor$ is the maximum integer less than M/β, and $\Lambda_{M \times N} = 0$ when $M > \lfloor M/\beta \rfloor$. Equations (22–38) are used to suppress the components $c[m], a_{M \times N}, q_{M \times N}$, and $g_{M \times N}. z_{M \times N}$ can be removed when there are no motions in the detection area. The resulting ideal signal is then
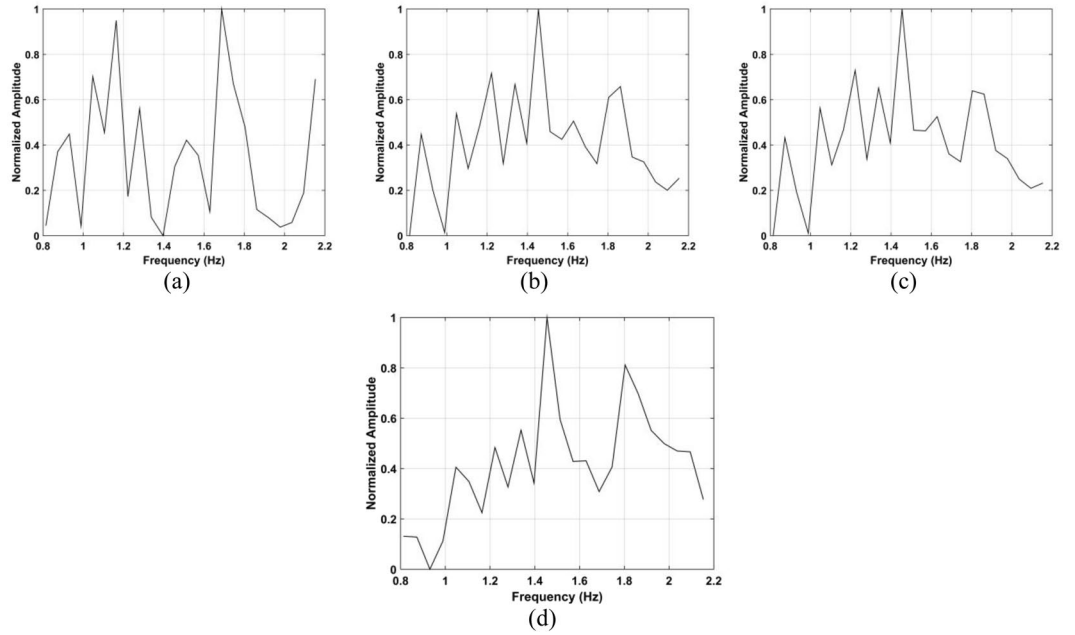
Figure 21. Clutter suppression results using the (**a**) FFT, (**b**) CSD, (**c**) LCSD, and (**d**) DLCSD methods.
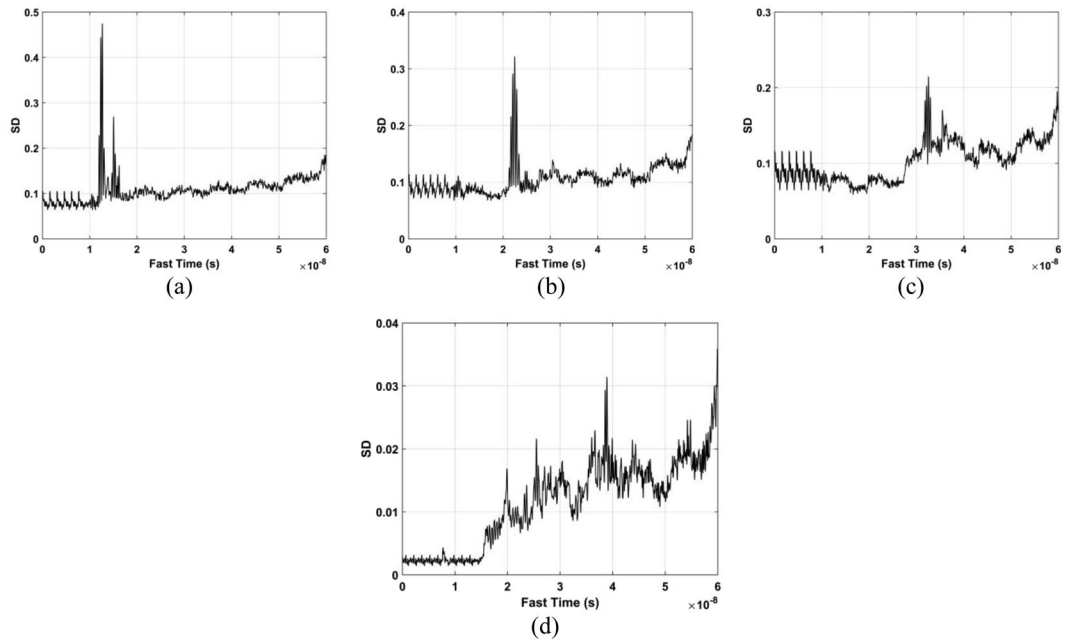
Figure 22. The SD with the actuator indoors located (**a**) 4 m, (**b**) 7 m, (**c**) 10 m, and (**d**) 12 m from the radar.

$$\begin{aligned} \Psi[m, \ n] &= a_v s(m\delta_T - \tau_v(nT_s)) \\ &= a_v s(m\delta_R - v\tau_v(nT_s)) = h[m, \ n] \end{aligned} \tag{39}$$

Range Determination. The standard deviation (SD) of the received pulses is used for range estimation of human subject. The SD for fast-time index m is[45]

$$\Gamma[m] = \sqrt{\frac{\sum_{n=1}^{N}(\Psi[m, n] - \mu_m)^2}{N - 1}} \tag{40}$$
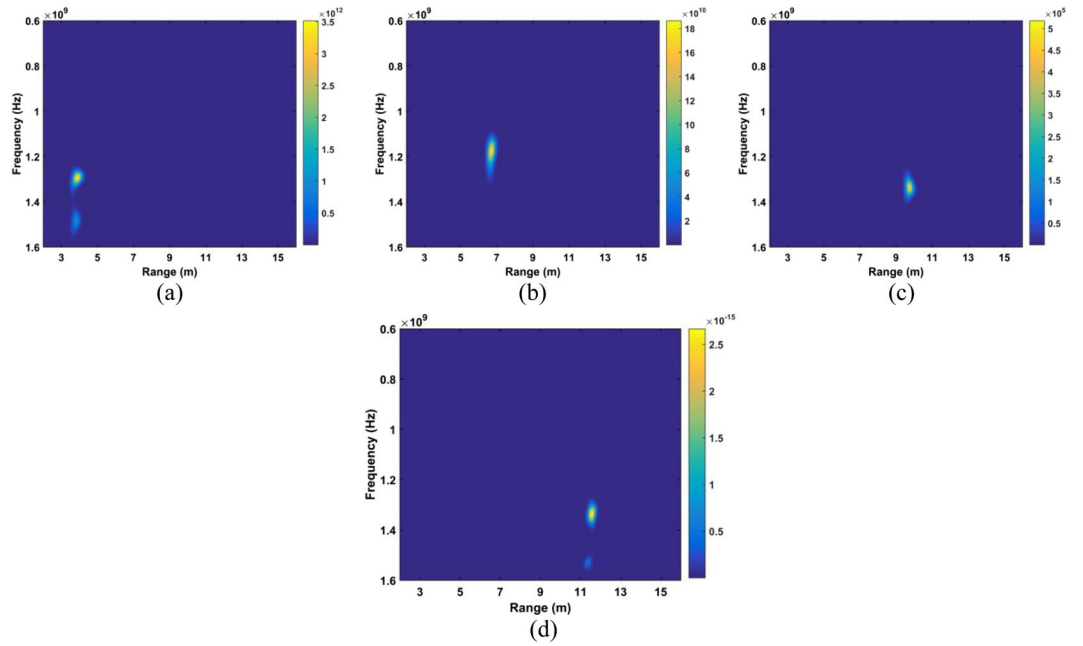
Figure 23. Range estimation using the proposed method with the actuator located (**a**) 4 m, (**b**) 7 m, (**c**) 10 m, and (**d**) 12 m from the radar.

Figure 24. Actuator frequency estimation using the (**a**) proposed, (**b**) CSD, (**c**) LCSD, and (**d**) FFT methods.

where μ_m is the mean. The data from a female volunteer at 9 m far from the radar were used for SD calculation in through-wall conditions, and Fig. 4 gives the results. This figure shows that the SD is large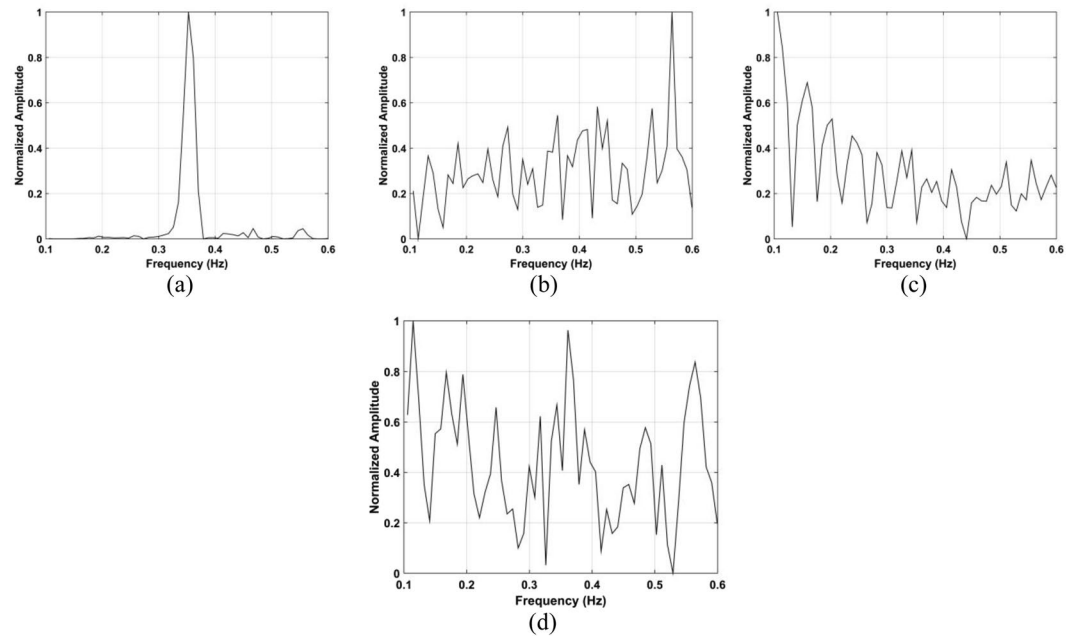 when a subject is present, which indicates that it can be used for the detection of vital sign signals. Figure 5 shows the corresponding spectrums obtained from the SD values in the target area using an FT, which indicates the SD is periodic, and thus can be used for range estimation.

The DSFT of (40) is used for analyzing signal characteristics in time-frequency domain[46,47]. Windowing is also employed, which gives

$$K[o, \ p] = \sum_{m=1}^{M} \Gamma[m] \Xi[o - m] e^{-j2p\pi m/\mathbf{P}},$$

(41)
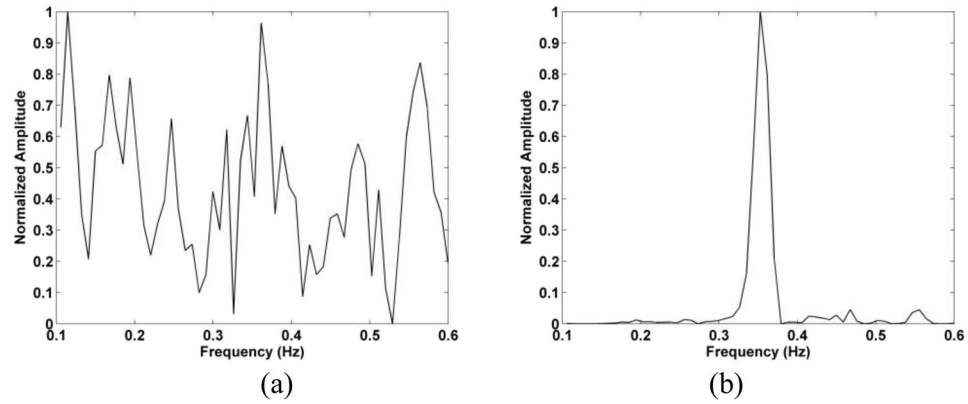
Figure 25. Frequency estimation with the actuator located 11 m from the radar using the (**a**) FFT and (**b**) proposed methods.

where p represents frequency and Ξ represents the used Hamming window which is expressed as

$$\Xi(o) = \alpha - \beta \cos\left(\frac{2\pi o}{O}\right), \quad o = 0, \ 1, \ \cdots, \ O, \tag{42}$$

where $\alpha = 0.54$ and $\beta = 0.46$. The DSFT window length must be chosen carefully. If it is too small, there will be excessive, and the result tends to zero length increases. A window of $O = 512$ was chosen based on extensive simulation results. The DSFT is shown in Fig. 6 and has a range error of only 0.104 m. Figure 7 shows the calculated SD values and the corresponding spectrums using DSFT without a human subject in the environment. Compared Figs 6 with 7(b), result indicates that the range information can be acquired by employing the DSFT technique, which is given by

$$\widehat{L} = \frac{v\hat{\tau}}{2} \tag{43}$$

where $\hat{\tau}$ denotes the time delay, i.e. the peak value from (39).

Frequency Estimation.   The time index for the delay estimate $\hat{\tau}$ is

$$\Im = \hat{\tau}/\delta_T. \tag{44}$$

To estimate the vital sign signal frequencies, an FT is performed on (39), which gives

$$Y(v, \ t) = a_v S(v) e^{-j2\pi v \tau_v(t)}. \tag{45}$$

Using the time index in (44), (45) can be given by

$$Y(\Im, \ t) = a_v S\left(\frac{\Im}{\delta_T}\right) e^{-j2\pi \frac{\Im}{\delta_T} \tau_v(t)}, \tag{46}$$

and taking the logarithm gives[4]

$$ln[Y(\Im, \ t)] = ln(a_v) + ln\left[S\left(\frac{\Im}{\delta_T}\right)\right] - j2\pi \frac{\Im}{\delta_T} \tau_v(t) + j2k\pi, \tag{47}$$

where the term $j2k\pi$ represents the phase variation due to any non-static objects and k is an integer. The unwrapping method can be used to remove this term[20], but differentiation provides a simpler solution[16]. The imaginary part of (47) includes the phase variation of the vital signs $j2\pi \frac{\Im}{\delta_T} \tau_v(t)$. Compared with the approach in Section II, the products of the vital signs and the harmonics are not as significant when only the phase is considered. Further, differentiating the logarithm term is simple and straightforward, making this method suitable for real-time vital sign detection[16]. Using (3), the result is

$$\lambda' = 4\pi^2 \frac{\Im}{\delta_T}[f_r \tau_r \cos(2\pi f_r t) - f_h \tau_h \sin(2\pi f_h t)] \tag{48}$$

where $\prime$ denotes differentiation, and the corresponding discrete form as

$$\lambda'[n] = 4\pi^2 \frac{\Im}{\delta_T}[f_r \tau_r \cos(2\pi f_r n T_s) - f_h \tau_h \sin(2\pi f_h n T_s)] \tag{49}$$

The respiration frequency is typically 0.2 Hz to 0.5 Hz with an amplitude of 5 to 15 mm, and the heart rate is 0.8 Hz to 2.5 Hz with an amplitude of 2 to 3 mm[38]. The SNCR can thus be improved using a window for these frequencies. A rectangular window with length κ in the frequency domain is employed for each slow-time dimension which gives

$$\Sigma[n] = \chi[n] \odot \text{FFT}\{\lambda'[n]\}, \quad n = k^*, \ k^* + 1, \ \dots, \ k^* + \kappa - 1 \tag{50}$$

where $\odot$ is the window operator and k^* is the minimum index. The FA method proposed in[48] is employed to suppress any remaining clutters existing in vital sign signals in the same frequency band. This gives

$$\mathbf{\dot{a}}[n] = l[n] + jl[n] \tag{51}$$

where

$$l[n] = \begin{cases} 2\Sigma[n], & n > 0 \\ \Sigma[n], & n = 0 \\ 0, & n < 0 \end{cases} \tag{52}$$

Performance Results

Compared with several well-known techniques, the detection capability of the presented algorithm is tested in this section. This is achieved using experimental results obtained in both indoor and outdoor environments.

Experimental Setup. Figure 8 shows the UWB radar experimental setup. The wall has a thickness of 100 cm and is composed of brick (30 cm), reinforced concrete (40 cm), and wood (30 cm). The four experiments described below were conducted to obtain data for performance evaluation.

1. This experiment was carried out at IECAS outdoors as shown in Fig. 9(a). A female subject stood breathing normally and facing the radar. The subject stood at 11 m, 9 m, 6 m, and 3 m far from the radar successively. The radar was placed on a table at a height of 1.5 m.
2. This experiment was conducted indoors at the China National Fire Equipment Quality Supervision Center (CNFEQSC) as shown in Fig. 9(b). A male subject stood 12 m, 10 m, 7 m, and 4 m far from the radar. The radar was placed on a table at a height of 1.3 m.
   An actuator was used instead of a human subject in experiments 3 and 4. The actuator moves at a frequency of 0.3333 Hz with an amplitude of 3 mm.
3. This experiment was carried out at IECAS outdoors as shown in Fig. 10(a). The actuator was placed on a table at a height of 1.3 m at a distance of 11 m from the radar.
4. This experiment was conducted at CNFEQSC indoors as shown in Fig. 10(b). The actuator was placed 12 m, 10 m, 7 m, and 4 m far from the radar.

The performance of the proposed, FFT, constant false alarm ratio (CFAR)[34], and MHOC[37] methods as well as the advanced method (AM)[36], the FA method with different times, and the CSD[42] and logarithm CSD (LCSD) techniques are evaluated in the following sections using the experimental data.

Initial Detection Performance. In this subsection, based on the data from experiment 1, the performance of the clutter suppression steps is considered with the subject 9 m from the radar. The results after removing the DC component and static clutter are given in Fig. 11(a,b), respectively, and Fig. 11(c) presents the results after removing the linear trend. These figures show that human respiration signals are quite weak and as a consequence, the oscillations are challenging to determine. The results after SVD and fast-time filtering are given in Fig. 11(d,e), respectively. These show a further reduction in the clutter which improves the respiration signal. Figure 11(f) shows the results after slow-time filtering and indicates that the respiration signal is significantly improved compared to the received signal in Fig. 2.

Human Subject Detection Outdoors. In this subsection, the data from experiment 1 is used for evaluating the performance of the detection method. Usually, the SNR of vital signs increases with decreasing distance between the radar and human subject due to large-scale attenuation[32]. The improvement in SNR can thus be used to evaluate the performance, which can be obtained as

$$SNR = 20 \log_{10} \left(\frac{\sum_{n=\mu_r-1}^{\mu_r+1} |\mathbf{\dot{a}}[n]|}{\sum_{n=\gamma_1}^{\mu_r-2} |\mathbf{\dot{a}}[n]| + \sum_{n=\mu_r+2}^{\gamma_2} |\mathbf{\dot{a}}[n]|} \right), \tag{53}$$

where μ_r is the frequency index corresponding to the target, and γ_1 and γ_2 are the boundaries of the frequency window.

The data sets acquired outdoors were used to evaluate four detection methods. Figure 12 gives the calculated SD results and the corresponding spectrums using the DSFT technique are shown in Fig. 13. The errors in the estimations of range information are 26 cm, 11 cm, 5 cm, and 5 cm at ranges of 11 m, 9 m, 6 m and 3 m, respectively.

Table 1 gives the estimations of human respiration frequency, range errors, and SNR values from (53) for four detection algorithms. This shows that the presented method supplies the most accurate range estimates and high SNR, particularly for long distances. At a distance of 11 m, the SNR with the proposed method is 3.25 dB while the SNR is only −15.3 dB with the CFAR method, a difference of 18.6 dB. The respiration frequency estimates using the proposed method are 0.26 Hz at 11 m, 0.29 Hz at 9 m, 0.26 Hz at 6 m, and 0.32 Hz at 3 m, respectively, which are considerably more accurate than with the other methods. Figure 14 gives the results acquired from the CFAR technique, which indicate that the range information cannot be estimated accurately with this method over long distances. Figure 14(b–d) show that there remains significant clutter at distances of 6 m or more.

To evaluate the heart rate estimation performance, the data with a male subject outdoors was used. A typical resting heart rate is 75 to 81 beats per minute, corresponding to frequencies of 1.25 to 1.35 Hz. Figure 15 shows that the heart rate estimates for the proposed method are 1.34 Hz, 1.34 Hz, and 1.45 Hz, respectively. It was not possible to obtain estimates using the CFAR method. The corresponding SNR values for the proposed and CFAR methods are given in Table 2. This shows that the proposed method provides a significant SNR improvement over the CFAR method as the smallest difference is 9.43 dB at a distance of 6 m. The very low SNR values for the CFAR method are the reason the heart rate could not be estimated.

Human Subject Detection Indoors. The data from experiment 2 is now used for evaluating the detection performance. Figure 16 shows the calculated SD values with the proposed method and the DSFT results are given in Fig. 17. The range estimates are 11.8 m, 9.89 m, 6.95 m, and 4.06 m for distances of 12 m, 10 m, 7 m and 4 m, respectively, and show that the range information can be estimated more accurately indoors. This is because it is a controlled environment which lacks factors such as wind. The respiration frequency estimation results are shown in Fig. 18. The estimates of for the four distances are 0.26 Hz, 0.29 Hz, 0.26 Hz, and 0.32 Hz.

Clutter Suppression. The capability of removing clutters was evaluated using the data from experiment 1 at 6 m. The harmonics and the products of the vital sign signals were suppressed using the FA method and the results are given in Figs 19 and 20. This shows that the four-FA method can supply a better SNR improvement than the FFT, two-FA, and one-FA methods. Table 3 gives the SNR values and shows that the additional improvement is minimal when the FA method is performed six times. The SNR for the FFT, CSD, logarithm CSD (LCSD) and differentiated LCSD (DLCSD) methods is also given in Table 4. The corresponding frequency domain results for the CSD, LCSD, and DLCSD methods are given in Fig. 21(b–d), respectively. The range estimation results in Fig. 14 show that these methods do not effectively suppress the clutter compared to the proposed method.

Actuator Experiment Results. The data from the conducted actuator experiments were used for testing the presented algorithm. The actuator was used to imitate human respiration with the amplitude of 3 mm and a frequency of 0.3333 Hz and. Figure 22 shows the SD values for the proposed method using the data from experiment 4 and the corresponding range and frequency estimation results are given in Figs 23 and 24, respectively. The frequency estimate from Fig. 24(a) is 0.353 Hz. The frequency estimate using the CSD method from Fig. 24(b) is 0.11 Hz and the estimate using the LCSD method from Fig. 24(c) is 0.56 Hz. The FFT method provides the worst performance as the frequency estimate from Fig. 24(d) is 0.12 Hz. Compared with the actual frequency of 0.3333 Hz, the proposed method provides the best estimate with an error of only 0.019 Hz. The frequency estimates using the outdoor data from experiment iii is shown in Fig. 25. The frequency estimates and corresponding deviations are given in Table 4 for three trials of the experiment. All these results indicate that the presented algorithm has the smallest deviation and significantly outperforms the other algorithms.

Conclusion

Vital sign detection was considered in this paper for applications such as after a natural disaster. The respiration and heartbeat frequencies were estimated using an impulse UWB radar. The CSD-based FA method was shown to be effective in suppressing signal products and harmonics. The discrete short-time Fourier transform (DSFT) of the calculated standard deviation (SD) values was used to estimate the range information of the volunteer. Experimental data obtained using a UWB radar were used to evaluate the performance of several techniques. The results obtained indicate that the proposed method can more effectively remove clutter and improve the SNR than the other methods. Further, it provides better range and frequency estimates[49–53].

Availability of Data and Materials
All data analyzed during this study are included in this paper.

References

1. Liang, S. D. Sense-through-wall human detection based on UWB radar sensors. *Signal Process.* **126**, 117–124 (2016).
2. Muqaibel, A. H., Abdalla, A. T., Alkhodary, M. T. & Alawsh, S. A. Through-the-wall radar imaging exploiting Pythagorean apertures with sparse reconstruction. *Digit. Signal Process.* **61**, 86–96 (2017).
3. Stanciu, M. I., Azou, S., Rădoi, E. & Şerbănescu, A. A Statistical analysis of multipath interference for impulse radio UWB systems. *J. Franklin. I.* **352**, 5952–5967 (2014).
4. Wang, J. *et al.* Noncontact distance and amplitude-independent vibration measurement based on an extended DACM algorithm. *IEEE Trans. Instrum. Meas.* **63**, 145–153 (2014).
5. Singh, A., Gao, X., Yavari, E. & Zakrzewski, M. Data-based quadrature imbalance compensation for a CW Doppler radar system. *IEEE Trans. Microw. Theory Techn.* **61**, 1718–1724 (2013).
6. Wang, G., Gu, C., Inoue, T. & Li, C. A hybrid FMCW-interferometry radar for indoor precise positioning and versatile life activity monitoring. *IEEE Trans. Microw. Theory Techn.* **62**, 2812–2822 (2014).
7. Mercuri, M., Soh, P. J., Boccia, L. & Schreurs, D. Optimized SFCW radar sensor aiming at fall detection in a real room environment. *in Proc. IEEE Biomed. Wireless Technol. Netw. Sens. Syst.*, Austin TX USA, 4–6 (2013).

8. Mercuri, M., Ping, J. S., Pandey, G. & Karsmakers, P. Analysis of an indoor biomedical radar-based system for health monitoring. *IEEE Trans. Microw. Theory Techn.* **61**, 2061–2068 (2013).

9. Muqaibel, A. & Safaai-Jazi, A. Characterization of wall dispersive and attenuative effects on UWB radar signals. *J. Franklin I.* **345**, 640–658 (2008).

10. Wang, Y., Liu, Q. & Fathy, A. E. Simultaneous localization and respiratory detection of multiple people using low cost UWB biometric pulse Doppler radar sensor. *in IEEE MTT-S Int. Microw. Symp. Dig.*, Montreal QC Canada (2012).

11. Wang, Y., Liu, Q. & Fathy, A. E. CW and pulse–Doppler radar processing based on FPGA for human sensing applications. *IEEE Trans. Geosci. Remote Sens.* **51**, 3097–3107 (2013).

12. Koo, Y. S., Ren, L., Wang, Y. & Fathy, A. E. UWB MicroDoppler radar for human gait analysis, tracking more than one person, and vital sign detection of moving persons. In *IEEE MTT-S Int. Microw. Symp. Dig.*, Seattle WA USA, 1–4 (2013).

13. Nijsure, Y., Tay, W. P., Gunawan, E. & Wen, F. An impulse radio ultrawideband system for contactless noninvasive respiratory monitoring. *IEEE Trans. Biomed. Eng.* **60**, 1509–1517 (2013).

14. Li, J., Liu, L. & Zeng, Z. Advanced signal processing for vital sign extraction with applications in UWB radar detection of trapped victims in complex environments. *IEEE J. Sel. Topics Appl. Earth Observat. Remote Sens.* **7**, 783–791 (2014).

15. Li, Z., Li, W. & Lv, H. A novel method for respiration-like clutter cancellation in life detection by dual-frequency IR-UWB radar. *IEEE Trans. Microw. Theory Techn.* **61**, 2086–2092 (2013).

16. Hu, W. *et al.* Noncontact accurate measurement of cardiopulmonary activity using a compact quadrature Doppler radar sensor. *IEEE Trans. Biomed. Eng.* **61**, 725–735 (2014).

17. Gu, C. & Li, C. Assessment of human respiration patterns via noncontact sensing using doppler multi-radar system. *Sensors* **15**, 6383–6398 (2015).

18. Lazaro, A., Girbau, D. & Villarino, R. Techniques for clutter suppression in the presence of body movements during the detection of respiratory activity through UWB radars. *Sensors* **14**, 2595–2618 (2014).

19. Chuantao, L. *et al.* A method for remotely sensing vital signs of human subjects outdoors. *Sensors* **15**, 14830–14844 (2015).

20. Ren, L., Kooet, Y., Wang, Y. & Fathy, A. Noncontact multiple heartbeats detection and subject localization using UWB impulse doppler radar. *IEEE Microw. Wirel. Compon. Lett.* **25**, 690–692 (2015).

21. Vu, V. T., Sjogren, T. K., Pettersson, M. I. & Gustavsson, A. Detection of moving targets by focusing in UWB SAR theory and experimental results. *IEEE Trans. Geosci. Remote Sens.* **48**, 3799–3815 (2010).

22. Zhuge, X. & Yarovoy, A. A sparse aperture MIMO-SAR based UWB imaging system for concealed weapon detection. *IEEE Trans. Geosci. Remote Sens.* **49**, 509–518 (2011).

23. Ascione, M., Buonanno, A., D'Urso, M. & Angrisani, L. A new measurement method based on music algorithm for through-the-wall detection of life signs. *IEEE Trans. Instrum. Meas.* **62**, 13–26 (2013).

24. Liu, L., Liu, Z. & Barrowes, B. Through-wall bio-radiolocation with UWB impulse radar-observation, simulation and signal extraction. *IEEE J. Sel. Topics Appl. Earth Observ. Remote Sens.* **4**, 791–798 (2011).

25. Liu, L. *et al.* Numerical simulation of UWB impulse radar vital sign detection at an earthquake disaster site. *Ad Hoc Netw.* **13**, 34–41 (2014).

26. Baldi, M. *et al.* Non-invasive UWB sensing of astronauts' breathing activity. *Sensors* **15**, 565–591 (2015).

27. Li, Z., Li, W., Lv, H. & Zhang, Y. A novel method for respiration-like clutter cancellation in life detection by dual-frequency IR-UWB radar. *IEEE Trans. Microw. Theory Technol.* **5**, 2086–2092 (2013).

28. Liang, X. *et al.* An improved algorithm for through-wall target detection using ultra-wideband impulse radar. *IEEE Access* **5**, 22101–22118 (2017).

29. Conte, E., Filippi, A. & Tomasin, S. ML period estimation with application to vital sign monitoring. *IEEE Signal Process. Lett.* **17**, 905–908 (2010).

30. Nezirovíc, A., Yarovoy, A. & Ligthart, L. P. Signal processing for improved detection of trapped victims using UWB radar. *IEEE Trans. Geosci. Remote Sens.* **48**, 2005–2014 (2010).

31. Liang, X. *et al.* Through-wall Human Being Detection Using UWB Impulse Radar. *EURASIP J Wirel Comm* **2018**, 1–17 (2018).

32. Liang, X. *et al.* Improved denoising method for through-wall vital sign detection using UWB impulse radar. *Digit. Signal Process* **74**, 72–93 (2018).

33. Zhang, Z. Human-target detection and surrounding structure estimation under a simulated rubble via UWB radar. *IEEE Trans. Geosci. Remote Sens.* **10**, 328–331 (2013).

34. Xu, Y., Wu, S., Chen, C. & Chen, J. A novel method for automatic detection of trapped victims by ultrawideband radar. *IEEE Trans. Geosci. Remote Sens.* **50**, 3132–3142 (2012).

35. Xie, Y. & Fang, G. Equi-amplitude tracing algorithm based on base-band pulse signal in vital sign detecting. *Electron. Inf. Technol.* **31**, 1132–1135 (2009).

36. Liang, X. *et al.* Ultra-wide band impulse radar for life detection using wavelet packet decomposition. *Phys Commun-Amst* **29**, 31–47 (2018).

37. Xu, Y., Dai, S., Wu, S. & Chen, J. Vital sign detection method based on multiple higher order cumulant for ultra-wideband radar. *IEEE Trans. Geosci. Remote Sens.* **50**, 1254–1265 (2012).

38. Hu, X. & Jin, T. Short-range vital signs sensing based on EEMD and CWT using IR-UWB radar. *Sensors* **16**, 2025, https://doi.org/10.3390/s16122025 (2016).

39. Li, C. & Lin, J. Random body movement cancellation in Doppler radar vital sign detection. *IEEE Trans. Microw. Theory Techn.* **56**, 3143–3152 (2008).

40. Park, B. K., Boric-Lubecke, O. & Lubecke, V. M. Arctangent demodulation with DC offset compensation in quadrature Doppler radar receiver systems. *IEEE Trans. Microw. Theory Techn.* **55**, 1073–1079 (2007).

41. Naishadham, K. & Piou, J. E. A robust state space model for the characterization of extended returns in radar target signatures. *IEEE Trans. Antennas Propag.* **56**, 1742–1751 (2008).

42. Ren, L. *et al.* Phase-based methods for heart rate detection using UWB impulse Doppler radar. *IEEE Trans. Microw. Theory* **64**, 3319–3331 (2016).

43. Hu, J., Zhu, G., Jin, T. & Zhou, Z. Adaptive Through-wall indication of human target with different motions. *IEEE Geosci. Remote Sens. Lett.* **11**, 911–915 (2013).

44. Mak, J. C. C., Bois, A. & Poon, J. K. S. Programmable multiring Butterworth filters with automated resonance and coupling tuning. *IEEE J. Sel. Top. Quant.* **22**, 1–9 (2016).

45. Liang, X., Zhang, H., Lv, T. & Gulliver, T. A. Energy detector based TOA estimation for MMW systems using machine learning. *Telecommun. Syst.* **64**, 417–427 (2017).

46. Allen, B. Short term spectral analysis, synthesis, and modification by discrete Fourier transform. *IEEE Trans. Audio Speech* **25**, 235–238 (1977).

47. Wojcicki, K., Milacic, M., Stark, A. & Lyons, J. Exploiting conjugate symmetry of the short-time Fourier spectrum for speech enhancement. *IEEE Signal Process. Lett.* **15**, 461–464 (2008).

48. Marple, L. Computing the discrete-time "analytic" signal via FFT. *IEEE Trans. Signal Process.* **47**, 2600–2603 (1999).

49. Huang, M. C. *et al.* A self-calibrating radar sensor system for measuring vital signs. *IEEE Trans. Biomed. Circuits Syst.* **10**, 352–363 (2016).

50. JalaliBidgoli, F., Moghadami, S. & Ardalan, S. A compact portable microwave life-detection device for finding survivors. *IEEE Embedded Syst. Lett.* **8**, 10–13 (2016).
51. Gennarelli, G., Ludeno, G. & Soldovieri, F. Real-time through-wall situation awareness using a microwave Doppler radar sensor. *Remote Sens.* **8**, 621, https://doi.org/10.3390/rs8080621 (2016).
52. Le, C., Dogaru, T., Nguyen, L. & Ressler, M. A. Ultra-wideband radar imaging of building interior: Measurements and predictions. *IEEE Trans. Geosci. Remote Sens.* **47**, 1409–1420 (2009).
53. Huang, Q., Qu, L. & Fang, G. UWB through-tall imaging based on compressive sensing. *IEEE Trans. Geosci. Remote Sens.* **48**, 1408–1415 (2010).

Acknowledgements

Author Contributions

All authors contributed to writing and editing this manuscript. X. Liang conceived and designed the experiments, performed the experiments, and analyzed the data. H. Zhang and T. Aaron Gulliver reviewed the results and revised the manuscript. J. Deng helped to update the resubmitted paper.

Additional Information

Competing Interests: The authors declare no competing interests.

Publisher's note: Springer Nature remains neutral with regard to jurisdictional claims in published maps and institutional affiliations.